Seeing at the SARA telescope: comparison with Tololo platform

Authors:*A. Tokovinin, E. Bustos, R. Rivera*
Version: 2
Date: 2024-10-24
File: prj/atm/smass/SARA/SARA-report.tex

Abstract. A portable seeing monitor based on RINGSS has been deployed at the SARA telescope from October 2023 to June 2024. Comparison of simultaneous turbulence profiles recorded by the regular Tololo RINGSS monitor and the portable RINGSS-2 at SARA shows the latter to measure a $0.1''$ worse seeing caused by the stronger ground-layer turbulence. This difference matters on nights with very good seeing. Dependence of turbulence parameters on the speed and direction of the ground wind is investigated.

Figure 1: The 6-m Halfmann tower with RINGSS-1 at the Tololo platform (left) and the RINGSS-2 instrument in a portable 3-m tower near SARA (right, image credit: C. Smither).

1 Introduction

The Blanco 4-m and several smaller telescopes were installed at the summit of Cerro Tololo in the 1960s and 1970s. CTIO also hosts a number of tenant telescopes operated by various external institutions and located on the northern slope of the main summit. The 60-cm SARA telescope (ex-Lowell installed in 1968) is sited a few hundred meters away to the South-East of the main summit (Fig. 2).

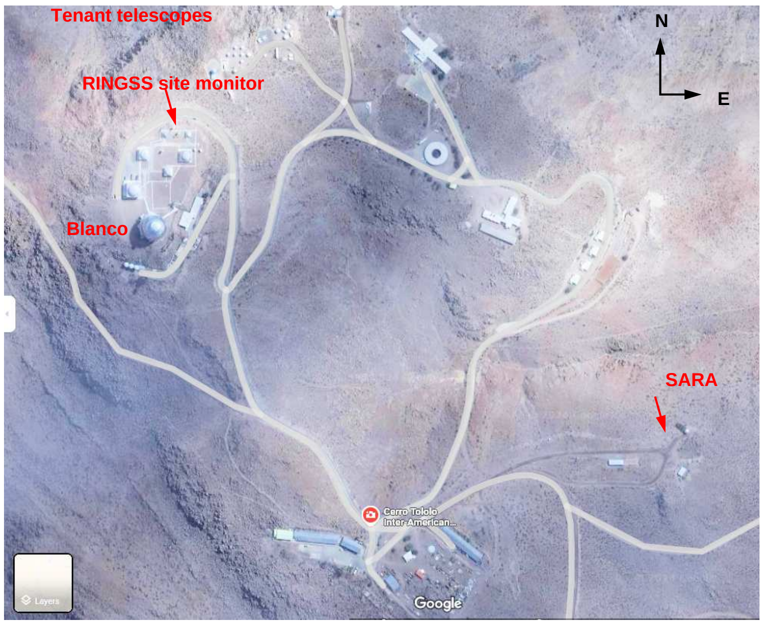

Figure 2: Satellite image of the Cerro Tololo summit in 2024 from Google maps. The red arrows show locations of the main Tololo RINGSS-1 site monitor and the portable RINGSS-2 near SARA.

Installation of new or upgrade of existing visitor telescopes requires knowledge of the seeing distribution on the summit. A prospect of upgrading the SARA telescope prompted characterization of its site with modern equipment. There is a broader interest in testing potential sites, particularly in the AURA domain at and around CTIO (e.g. Cerro Morado) as potential sites for new projects. This endeavor needs portable site monitors. Such systems are also mandatory for the study of new remote sites. A project of characterizing potential astronomical sites in the South-West of the US has been started by the NSF in 2019, but later abandoned. The seed funding of this project was used to develop and test a *Ring-Image Next Generation Scintillation Sensor* (RINGSS) instrument as a replacement of the more complex and technically obsolete MASS-DIMM instruments [1]. The first RINGSS system, originally developed as a prototype for this project, was permanently installed at Tololo in 2023 and eventually replaced the old MASS-DIMM; comparison of the overlapping data indicated a good mutual agreement [3].

A second RINGSS-2 instrument has been assembled at CTIO in 2022–23 for the study of other sites. Unlike RINGSS-1, it uses the alt-az mount configuration and a different enclosure. The RINGSS-2 instrument participated in the site-monitoring campaign at Paranal in March 2023 and demonstrated a very good agreement with other instruments [2]. That same instrument has been deployed at SARA in October 2023.

2 Instruments

The RINGSS turbulence monitors are based on the 5-inch Celestron Schmidt-Cassegrain telescope with a low-noise CMOS camera ASI290MM and small optics that transforms the stellar image into a ring and defines the spectral band-pass. Series of 2000 such rings with 1 ms exposure (data cubes) are acquired and processed online. Statistics of intensity fluctuations along the ring, averaged over 10 data cubes, is used to measure crude 8-layer turbulence profiles [1]. Alternative seeing estimate obtained from the distortions of the ring (DIMM-like) is computed as a check, but it is not used here (seeing is derived from the turbulence profile). Seeing in the free atmosphere corresponds to turbulence located at 500 m and above. RINGSS also measures the effective (turbulence-weighted) wind speed in the upper atmosphere from which the atmospheric time constant τ_0 is computed. All turbulence data here refer to the wavelength of 0.5 μm and observations at zenith.

The standard turbulence parameters such as seeing are defined in the framework of the Kolmorogov turbulence model and weak perturbations and are intrinsically approximate because this model differs from the reality [4]. Additional approximations are involved in measuring these parameters. The RINGSS instruments interpret their signals assuming weak wave-front distortions, so under very poor seeing the results become less accurate.

The RINGSS-1 instrument uses the compact harmonic-drive Rainbow Astro mount RST-135 in equatorial mode. The mount is attached to a solid tube pointing at the celestial pole and supported by a truss. A co-axial cylindrical enclosure, designed and built at CTIO [5], is part of the support structure. The instrument is attached atop the 6-m Halfmann tower that hosted previously the TMT site monitor which failed in 2012. The tower is located near the northern edge of the Tololo platform (Fig. 1, left).

The portable RINGSS-2 instrument uses identical RST-135 mount in the alt-az mode. The enclosure is a square box with two petals driven by commercial actuators [6]. A portable hexapod tower developed by R. Rivera is assembled from three V-shaped elements, bolted together and attached to three concrete pads in the ground (Fig. 1, right). Under a wind of 3 to 5 m/s, the stellar image moves with an rms amplitude of $0.4''$, with most power concentrated below 5 Hz and dominated by the atmospheric tilts (the jitter is isotropic). A small peak near 33 Hz (presumably the tower resonant frequency) is present. These vibrations have no effect on the instrument operation.

3 Data scope

RINGSS measures turbulence parameters with a typical cadence of 40 s. The results are appended to the text file and pushed to the CTIO environmental database. Each database record contains the following parameters: `time, star, zen, flux, see2, see, fsee, wind, tau0, theta0, totvar, erms, J0, J025, J05, J1, J2, J4, J8, J16`. Here `see` is the seeing derived from the turbulence profile, `see2` is the alternative seeing estimate from ring shape distortions, `fsee, wind, tau0` are the free-atmosphere (FA) seeing, effective wind speed, and atmospheric time constant τ_0, respectively. The eight numbers `J0` to `J16` are the turbulence integrals (in units of 10^{-13} m$^{1/3}$) in the 8 layers with fixed heights of 0, 0.25, 0.5,... 16 km. The parameter `erms` is the rms residual between measured and fitted statistical moments, in relative units; it quantifies how well the 8-layer profile matches the data. The strength of the scintillation (hence the validity of the small-perturbation approximation) is quantified by the relative flux variance `totvar`.

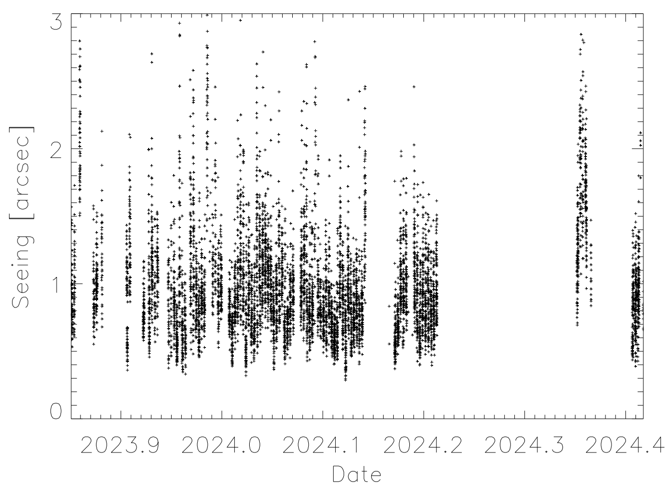

Figure 3: Seeing vs. date from the RINGSS-1 monitor at Tololo with simultaneous RINGSS-2 data. Every 10th point is plotted to reduce the overlap.

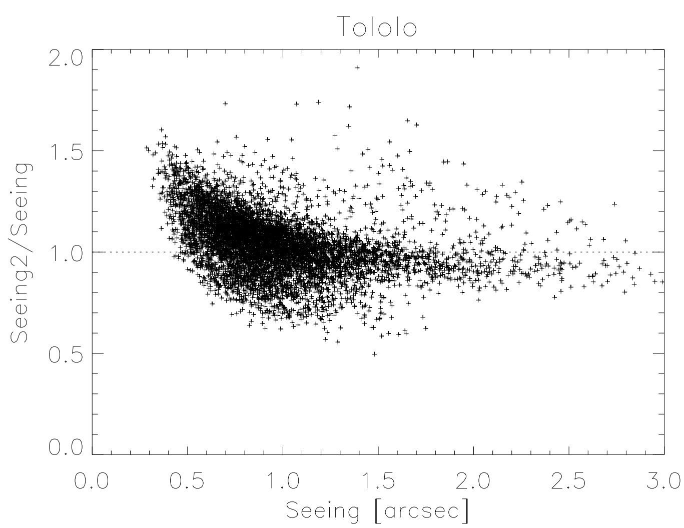

Figure 4: Ratio of the alternative seeing estimate `see2` to the scintillation-based estimate `see` at Tololo. Every 10th point is plotted.

The pixel scale is determined from images of suitable double stars. It is $1.78''$ and $1.57''$ for RINGSS-1 and RINGSS-2, respectively. The two instruments worked simultaneously for the first time on Nov. 11, 2023; RINGSS-2 stopped operation on June 2, 2024 for technical failure of its electronics. So, the data in common, used here, cover a half-year period. They were retrieved from the CTIO environmental database using SQL commands. The weather data from Tololo were queried using the web page `http://139.229.13.222/web/CTIO/tololo_weather_download.php`.

The text files retrieved from the database were ingested into IDL structures, with 127664 and 121121 elements for RINGSS-1 and -2, respectively. The two site monitors were matched in time within 1 min., leaving 76214 simultaneous measurements. The weather data exist for most (but not) all matched records. The matched data were filtered to remove glitches using the following criteria: seeing less than $3''$, `erms`< 0.3, and valid meteo data. There are 73117 filtered records.

Figure 3 illustrates the time coverage of this data set. Large gaps are caused by the technical downtime of one or other site monitor. The total time span is 0.567 yr. Figure 4 compares the alternative and main seeing estimates, as a health check. The median ratios of these estimates are 1.036 and 1.038 at Tololo and SARA, respectively, and the plot for SARA is similar. Under very good seeing, the estimate `see2` is systematically larger than `see`. This effect is present in all RINGSS data. Its origin is likely related to the optical imperfection of the ring image that translates into additional fluctuations of the ring shape, analogous to the bias in a defocused DIMM. The scintillation-based estimate `see` is more robust.

4 Results

4.1 Seeing

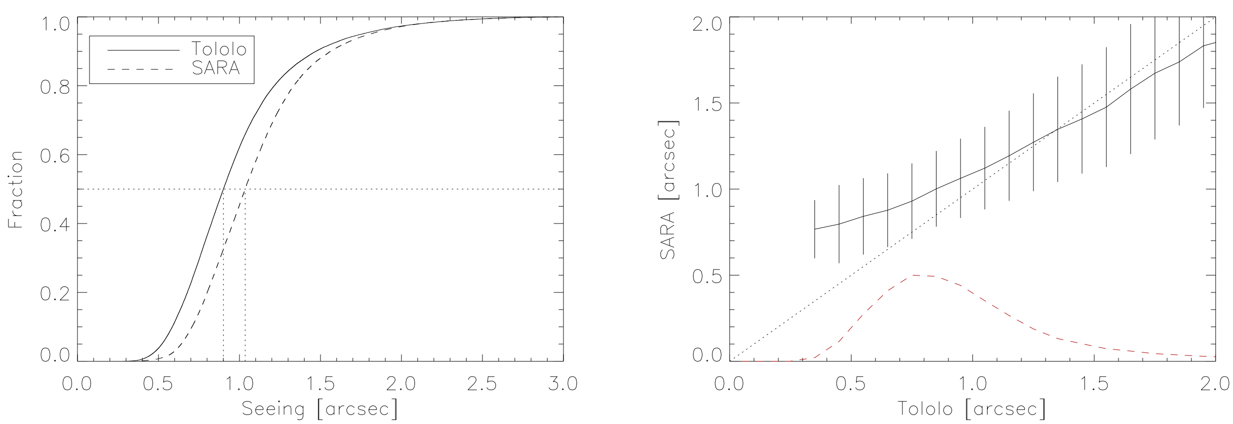

Figure 5: **Left:** Cumulative distribution of seeing. The vertical dotted lines show the median values of $0.901''$ and $1.035''$. **Right:** Seeing at SARA vs. seeing at Tololo in bins of $0.1''$. The solid line shows mean values, the bars are $\pm 1\sigma$ range, and the dotted line is a 1:1 relation. The red dashed curve shows the scaled histogram.

Figure 5, left, shows the cumulative histograms of simultaneous seeing measurements. The median values at Tololo and SARA are $0.901''$ and $1.035''$, respectively. Roughly speaking, the histogram at SARA is shifted to the right by $0.1''$, although the tails at bad seeing match well. The right-hand plot shows an XY comparison using binning (plotting all 71K points would be a mess). It is clear that the difference between the two sites increases under very good seeing.

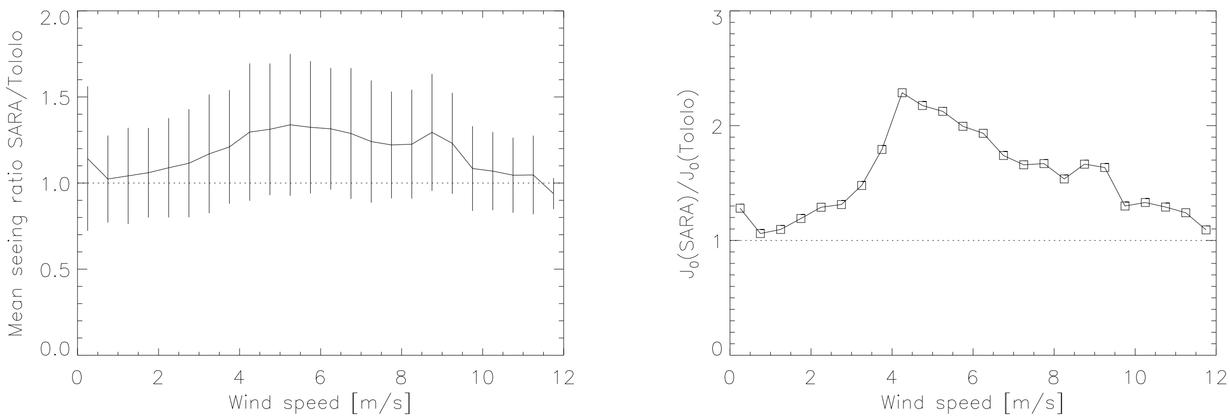

Figure 6: Dependence of the relative difference between SARA and Tololo on the wind speed, with bins of 0.5 m/s. **Left:** Mean ratio of seeing at SARA to the seeing at Tololo. The solid line plots the mean ratio, the vertical bars show the $\pm 1\sigma$ range. **Right:** Ratio of the mean ground-layer turbulence integrals J_0 at both sites.

Table 1: Dependence of median seeing on the wind direction

Parameter	North (300°–60°)	South (120°–240°)
Number of samples N	56842	12154
Median wind speed (m/s)	3.71	2.54
Median Tololo ($''$)	0.924	0.818
Median SARA ($''$)	1.057	0.954
J_0 Tololo (10^{-13} m$^{1/3}$)	3.04	2.61
J_0 SARA (10^{-13} m$^{1/3}$)	4.77	4.07

Figure 6 (left) explores the dependence of the ratio of seeing at two sites on the wind speed. Binning is used to eliminate the clutter and to get a more quantitative view. Interestingly, the seeing is similar at both slow and fast wind speeds, but deviates systematically at typical wind speeds of a few m/s. The right-hand panel shows the ratio of the ground-layer turbulence integrals at two sites binned by the wind speed. The dependence on the wind speed is even stronger; at winds between 4 and 6 m/s, the ground-layer turbulence at SARA is two times stronger than at Tololo. The ground-layer turbulence is comparable at slow and fast wind. The dependence of the median seeing on the wind direction is captured in Table 1. The northern wind (direction from 300° to 60°) is more frequent than the southern (from 120° to 240°) wind, and the wind in the east-west direction is even less common. At both sites there is a measurably better median seeing for the southern wind. The two lower lines of Table 1 contain the median turbulence integrals in the first (ground) layer J_0 (in units of 10^{-13}

$m^{1/3}$) computed for the two dominant wind directions. Clearly, the difference in seeing is caused by the different turbulence intensity in the ground layer. The median turbulence integrals in the higher layers do not show any dependence on the ground wind direction.

4.2 Free-atmosphere seeing and atmospheric time constant

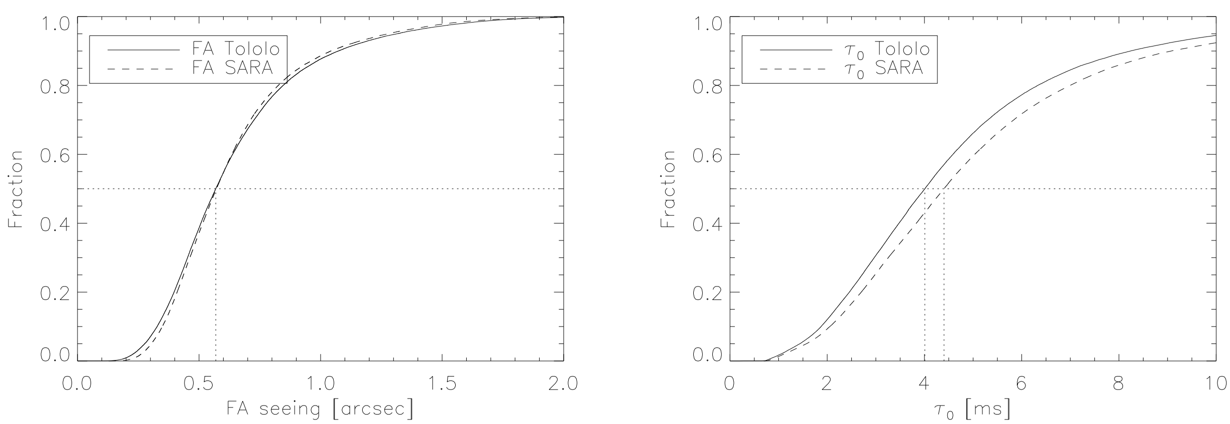

Figure 7: Cumulative histograms of the FA seeing (left) and τ_0 (right) at both sites.

Parameters of turbulence in the upper atmosphere should not depend on the site location within CTIO. As shown in Fig. 7, this is indeed the case. The median free-atmosphere (FA) seeing at Tololo and SARA is $0.569''$ and $0.571''$, respectively. The median values of τ_0 differ a bit more, 4.01 and 4.40 ms.

4.3 Turbulence profiles

Table 2: Turbulence profiles in 10^{-13} $m^{1/3}$

H	Tololo		SARA	
(km)	Median	Mean	Median	Mean
0	2.14	2.93	3.91	4.58
0.25	0.00	0.28	0.00	0.21
0.5	0.26	0.46	0.24	0.55
1	0.48	0.87	0.26	0.69
2	0.41	0.72	0.23	0.58
4	0.43	0.76	0.29	0.62
8	0.56	0.92	0.60	0.97
16	0.19	0.22	0.22	0.26

Individual turbulence profiles have a large diversity, complicating their comparison. Large turbulence spikes occur usually in one or two layers. Owing to the spikes, the median values are always

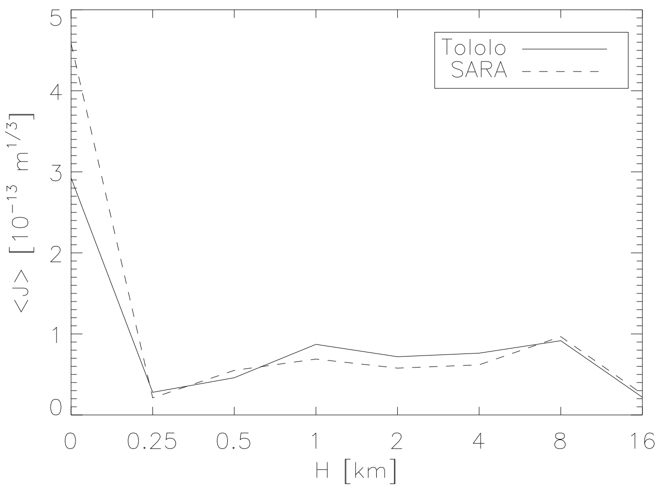

Figure 8: Mean turbulence profile at Tololo (solid line) and SARA (dashed line).

smaller than the mean. In the 0.25-km layer, the profiles typically have zero power, so the medians are also zero, while the mean values are not. The median and mean profiles are listed in Table 2, and the latter are plotted in Fig. 8. As expected, there is a very good agreement between all layers except the ground layer, where turbulence at SARA is systematically stronger than at Tololo. A seeing of $1''$ corresponds to the integral of $6.826 \cdot 10^{-13}$ m$^{1/3}$. The mean ground-layer integrals at Tololo and SARA thus correspond to the seeing of $0.60''$ and $0.79''$, respectively.

5 Discussion

In this study, we used two similar instruments based on the statistics of stellar scintillation. The statistical moments derived from the ring images are measured in absolute units. Their conversion into turbulence measurements (via weighting functions) uses the instrumental parameters such as pupil geometry, pixel scale, and conjugation height below the ground (or, equivalently, the ring radius), similarly to the MASS instrument. These parameters were carefully measured, so the results do not require any additional calibration. Comparison of both instruments side by side could be a health check, but it is not required. A good match of the upper-atmosphere parameters is by itself a check. Results of the Paranal campaign also validate the RINGSS instrument.

We found that the seeing at SARA is, on average, about $0.1''$ larger than at the Tololo platform. The difference is produced by the stronger ground layer, and it depends on the wind speed (Fig. 6). However, the monitor at SARA was installed at a lower height than at Tololo, contributing to this difference. Practically speaking, this result is encouraging for telescopes located at low height above ground, as is often the case for tenant facilities. The vertical resolution of RINGSS is insufficient for the study of the ground-layer turbulence profile; for such work, a lunar scintillometer would be an appropriate and simple instrument. This is why we recommend a combination of RINGSS with lunar scintillometer for the study of new sites.

The observers at Cerro Tololo and Cerro Pachón noted an unusually poor seeing in 2023–2024, including the period of this campaign. Indeed, the long-term statistics for Pachón suggests a median FA seeing of $0.40''$ [7], while we found a median of $0.57''$. Els et al. [8] found a median seeing at CTIO to be $0.79''$ (vs. $0.90''$ here) and noted the dependence of the ground-layer turbulence on the wind direction.

References

[1] Tokovinin, A. Measurement of turbulence profile from defocused ring images. 2021, MNRAS, 502, 794

[2] Griffiths, R., Bardou, L., Butterley, T., Osborn, J., Wilson, R., Bustos, E., Tokovinin, A., Le Louarn, M., Otarola, A. A comparison of next-generation turbulence profiling instruments at Paranal. 2024, MNRAS, 529, 320

[3] Tokovinin, A. Comparison between RINGSS and MASS-DIMM at Cerro Tololo. A. 2023 Feb 22, internal report.

[4] Tokovinin, A. The Elusive Nature of "Seeing". 2023, Atmosphere, 14, 1694

[5] Rivera, R., Bustos, E., Tokovinin, A. Enclosure of the RINGSS instrument. 2022, Jun 20, internal report.

[6] Tokovinin, A. Compact enclosure for the RINGSS site monitor. 2022, Nov. 3, internal report.

[7] Tokovinin, A., Travouilon, T. Model of optical turbulence prole at Cerro Pachón. 2006, MNRAS, 365, 1235.

[8] Els, S. G., Schöck, M., Bustos, E. et al. Four Years of Optical Turbulence Monitoring at the Cerro Tololo Inter-American Observatory (CTIO). 2009, PASP, 121, 922